Available online at www.sciencedirect.com
ScienceDirect
Journal of Power Sources 174 (2007) 668–672
JOURNAL OF POWER SOURCES
www.elsevier.com/locate/jpowsour

Short communication

In situ measurement of lithium mass transfer during charging and discharging of a Ni–Sn alloy electrode

Kei Nishikawa [a,*], Yasuhiro Fukunaka [a], Tetsuo Sakka [b], Yukio Ogata [b], J. Robert Selman [c]

[a] *Graduate School of Energy Science, Kyoto University, Yoshidahonmachi, Sakyo-ku, Kyoto 606-8501, Japan*
[b] *Institute of Advanced Energy, Kyoto University, Gokasyo, Uji 611-0011, Japan*
[c] *Center for Electrochemical Science and Engineering, Department of Chemical and Environmental Engineering, Illinois Institute of Technology, Chicago, IL 60616, USA*

Available online 3 July 2007

Abstract

The charging (lithiation) and discharging (delithiation) of a Ni–Sn alloy electrode was examined by means of holographic interferometry and laser scanning confocal microscopy (LSCM). The developing concentration profile of Li^+ ion during discharging (delithiation) of the Ni–Sn alloy electrode agreed reasonably well with the prediction based on transient diffusion theory, indicating that the cell configuration successfully suppressed natural convection due to the electrochemical reaction. The morphological variation of Ni–Sn alloy electrode during charge/discharge cycle could be observed very clearly by in situ LSCM. It was found that the contraction of active material during the discharge (delithiation) initiates cracks in the Ni–Sn alloy electrode.

Keywords: Ni–Sn alloy; Holographic interferometry; In situ LSCM; Concentration profile

1. Introduction

Lithium-ion batteries are widely used as power sources for portable electronic devices. In the future, they may be adopted also as power supply for the hybrid electric vehicle (HEV) and fully electric vehicle (EV). For applications such as HEV and EV, improvement of power density and cycle life is indispensable. At present, mainly graphite and graphitic materials are used for the anode in commercially available lithium-ion batteries. The coulombic capacity of these materials is practically limited by the theoretical capacity of graphite (372 mAh g^{-1}). Therefore, it is desirable to develop an alternative anode material.

The most promising alternative materials for the anode of a next-generation Li-ion battery are Sn-based or Si-based alloy materials [1–10]. The capacity of pure Sn metal is 994 mAh g^{-1}, assuming formation of $Li_{4.4}Sn$ alloy, however the volume change due to phase transformation exceeds 300%, relative to Sn metal, during charging and discharging. Thackeray et al. examined the possibility of Cu–Sn alloy from the viewpoint of crystal structure [2–4]. The electrochemical characteristics of this material have been reported by other groups [5,6]. Dahn et al. are systematically studying tin-based and Si-based alloys as anode candidate materials, using combinational techniques [7–9]. Mukaibou et al. proposed Ni–Sn alloy, in which the volume change is restricted by formation of a Ni matrix around the Sn atoms, and reported the electrochemical characteristic of this alloy [10]. They reported that charging and discharging caused cracks in the electrode, which indicates that the volume change is still significant or at least that the differential volume change during part of the cycle is excessive.

Our previous research focused on the ionic mass transfer of Li^+ ion near a lithium electrode during charging and discharging and its determination by in situ holographic interferometry [11–14]. From the viewpoint of lithium battery technology the ionic mass transfer phenomena in the electrolyte are especially relevant when fast charging and discharging takes place and lithium dendrite formation occurs. Also, the passivating layer called solid electrolyte interphase (SEI) is formed on the Li metal electrode, and this SEI plays a role in the occurrence of dendrite. However, even at low current density some remarkable phenomena were observed. In the case of a Li metal electrode, the start of the interference fringe shift indicating the onset of transient diffusion is noticeably delayed when electrolysis (charging, or lithiation) occurs at low current density. We have ascribed this

* Corresponding author.
E-mail address: nishikawa@inorg777.apchem.metro-u.ac.jp (K. Nishikawa).

0378-7753/$ – see front matter © 2007 Published by Elsevier B.V.
doi:10.1016/j.jpowsour.2007.06.241

to SEI formation [11–13] and correlated the time delay with the rate of SEI formation.

We have also studied, again by in situ holography, the transient concentration profile of Li^+ ion near an electrodeposited Ni–Sn alloy electrode during lithiation [14]. Differently from the Li metal electrode, the interference fringes begin to shift as soon as the electrolysis starts, and we ascribed this to the SEI layer at the interface between alloy material and electrolyte being much thinner than at a Li metal electrode.

From these studies we concluded that it is possible to analyze quantitatively the rate and extent of SEI formation at the metal/electrolyte interface from accurate measurement of transient liquid-phase concentration profiles during the charging process.

The purpose of the present study is to further examine the ionic mass transfer phenomena during discharging (delithiation) of a Ni–Sn alloy electrode in PC electrolyte. Two experiments are carried out to elucidate the interfacial phenomena. First, the development of the Li^+ concentration profile during discharge is compared with that observed at a Li metal electrode. Thus, the effect of the alloy electrode material is isolated. Second, the morphology of the lithiated thin-film alloy electrode is observed during charging and discharging by in situ LSCM. The electrode is monitored for the occurrence of cracks.

2. Experimental

A Ni–Sn thin-film was prepared by simultaneous electrodeposition of Ni and Sn on Cu foil from a pyrophoric acid bath of $NiCl_2{\cdot}6H_2O$ (0.075 M), $SnCl_2{\cdot}2H_2O$ (0.175 M), $K_4P_2O_7$ (0.5 M), glycine (0.125 M), and NH_4OH (5 mL L^{-1}). The temperature of the plating bath was maintained at 50 °C (323 K). The characterization of the electrodeposits was described in a previous paper [14]. The Ni–Sn thin-film electrode was used as the working electrode in the measurement described below. The electrolyte was propylene carbonate (PC) containing a predetermined concentration of 0.5 M $LiClO_4$ was used as received from Kishida Chemical Co. Ltd. Their analysis indicates the initial water content of the solution to be less than 30 ppm.

2.1. Holographic interferometry measurement

Lithium foil of 200 m thickness (Honjo Metal Co. Ltd.) was used for the reference electrode and counter electrode. The effective area of the working electrode was 10 mm × 6 mm. The working electrode and counter electrode surfaces were placed face to face, separated by a 2 mm thick electrolyte layer. Details of the electrolytic cell are as described in a previous paper [13]. The electrolytic cell was assembled in a glove box filled with highly pure Ar gas circulating continuously through molecular sieves 4 Å 1/16 (Nacalai Tesqu, Co. Ltd.) to remove water contaminant. The electrolytic cell was next horizontally installed in the holographic interferometer arrangement. The optical arrangement was as described earlier [11,12].

The electrolytic cell configuration was designed to eliminate as much as possible any natural convection due to the insertion of Li metal (depletion of Li^+ ion in the electrolyte) during charging, and the extraction of Li metal (enrichment in Li^+ ion of the electrolyte) during discharge. Therefore, the Ni–Sn alloy electrode was installed horizontally and facing downward during the insertion of Li in the Ni–Sn alloy, and upward during Li extraction. A constant current density of 0.3 mA cm^{-2} was applied to the Ni–Sn alloy electrode as a step function. This current density corresponds to about 0.5*C* rate in practical battery terminology.

2.2. LSCM measurement

The morphological history of the Ni–Sn electrode surface during lithiation and delithiation was in situ observed by LSCM. The cell design for this measurement is the same as that in the holographic interferometry described in (a), above. However, the configuration is such that the horizontally installed electrode surface faces upward in the electrolyte so that it can be observed directly by LSCM. The electrolytic cell body is of glass such as in a spectrophotometric cell. The distance between electrode surface and electrolytic cell wall was made as short as possible because the working distance of objective lens (LEICA, C PLAN L 40*x*/0.50) is rather short. The microscopic images were recorded by VHS video and analyzed later.

3. Results and discussion

3.1. Interferometric measurements

The main focus of this paper is the transient interference fringe pattern during the discharging (delithiation) of the lithiated Ni–Sn electrode. It is because cracks are suspected to occur during the discharge half-cycle of charge/discharge cycling. The transient behavior of the interference fringe pattern during charging (lithiation) was first measured with the lithiated Ni–Sn electrode. The electrolytic cell was then reinstalled upside down in the holographic interferometry arrangement and the transient fringe pattern during the discharge recorded as shown in Fig. 1. In both cases, the ionic mass transfer during the electrochemical reaction is governed by the one-dimensional transient diffusion equation with constant-flux boundary condition.

Fig. 1 shows that the interference fringe pattern before the start of electrolysis is perpendicular to the electrode. Once the electrolysis starts, the fringes start to shift immediately in both cases, insertion and extraction. The number of fringes shifted, *S*, can be converted to the refractive index in the electrolyte based on the interference equation

$$\Delta nd = S\lambda \tag{1}$$

where Δn is the difference of refractive index, d the optical path in the electrolytic cell, S the fringe shift, and λ is the wavelength of the laser beam (632.8 nm in this case). In a previous paper we reported the dependence of refractive index on the LiClO4 concentration, which is linear [12]. Therefore, Eq. (1) can be rewritten as

$$\Delta C = \left(\frac{\partial n}{\partial C}\right)\frac{S}{d} \tag{2}$$

where C is the concentration of $LiClO_4$.

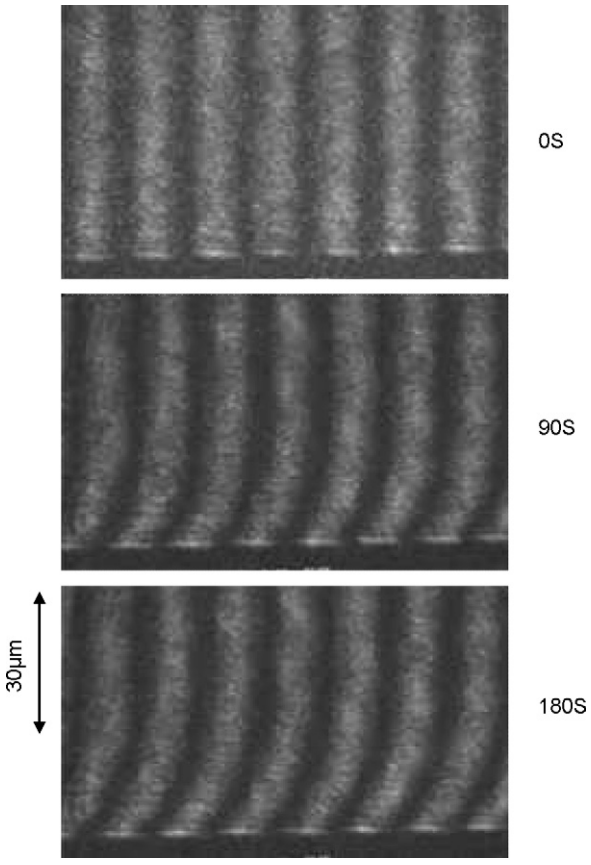

Fig. 1. Development of interference fringes during discharge (delithiation) of a Ni–Sn alloy electrode.

Using Eq. (2) the development of the surface concentration and the concentration boundary layer thickness with time, during the discharge of the Ni–Sn alloy electrode, are calculated. Fig. 2(a) demonstrates the change of electrode surface concentration of Li^+ ions, C_l^s, and Fig. 2(b) shows the development of concentration boundary layer thickness δ. The solid line represents the calculated C_l^s and δ based on the one-dimensional transient diffusion model, assuming constant-flux boundary condition [13,14]. The calculated curves are in reasonable agreement with the measured C_l^s and δ values, and this agreement is observed for the charging as well as the discharging process [14]. That is, the liquid-phase concentration profile during charging and discharging of a Ni–Sn alloy electrode with lithium can be understood from a simple one-dimensional transient diffusion model as long as the electrolytic cell configuration prevents the occurrence of natural convection.

3.2. LSCM measurement

Candidate alloys for negative electrode material of the Li-ion battery tend to undergo a large volume change during charging and discharging. Dahn et al. focus on Si–Sn alloys and examine the charging/discharging process by means of atomic force microscopy (AFM) and optical microscopy (OM). They reported measurements of the movement of active material particles during charging and discharging [15]. In this study, we

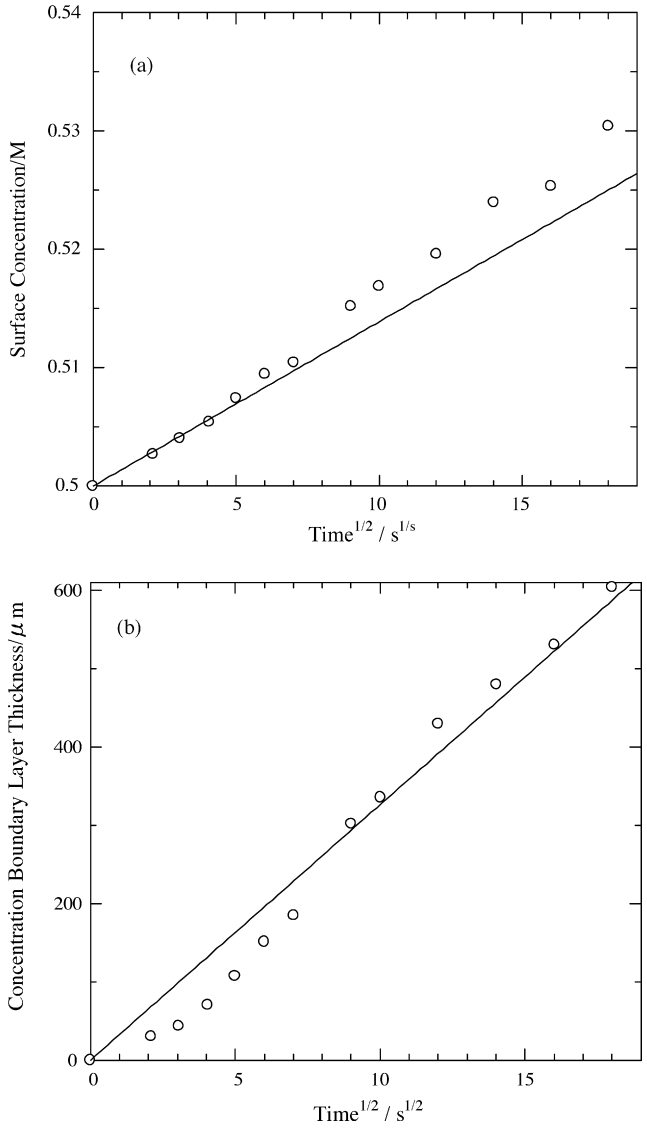

Fig. 2. Development of Li^+ ion surface concentration (a) and concentration boundary layer thickness (b) during delithiation of a Ni–Sn alloy electrode; C_l^s is surface concentration, δ is concentration boundary layer thickness.

apply LSCM to observe in situ the morphological variation of the Ni–Sn thin-film electrode during charging and discharging.

Fig. 3 illustrates the transient behavior of Ni–Sn surface morphology monitored by LSCM during a charging/discharging cycle. The letters besides the charge/discharge curve correspond to each of the LSCM images. Before charging, the electrode surface, shown in Fig. 3(a), has a smooth appearance, in agreement with the scanning electron microscopy (SEM) image in a previous paper [14]. In this case, the entire image area represents Ni–Sn alloy, i.e., the negative electrode material, prepared by electrodeposition. As charging (lithiation) proceeds, the brightness of the image decreases gradually (see Fig. 3(b and c)). The decay of the metallic luster indicates that the active material in the electrode surface become non-crystalline as the Ni–Sn substrate becomes progressively alloyed with Li. After the charging was practically complete, the electrolytic cell was left at rest for

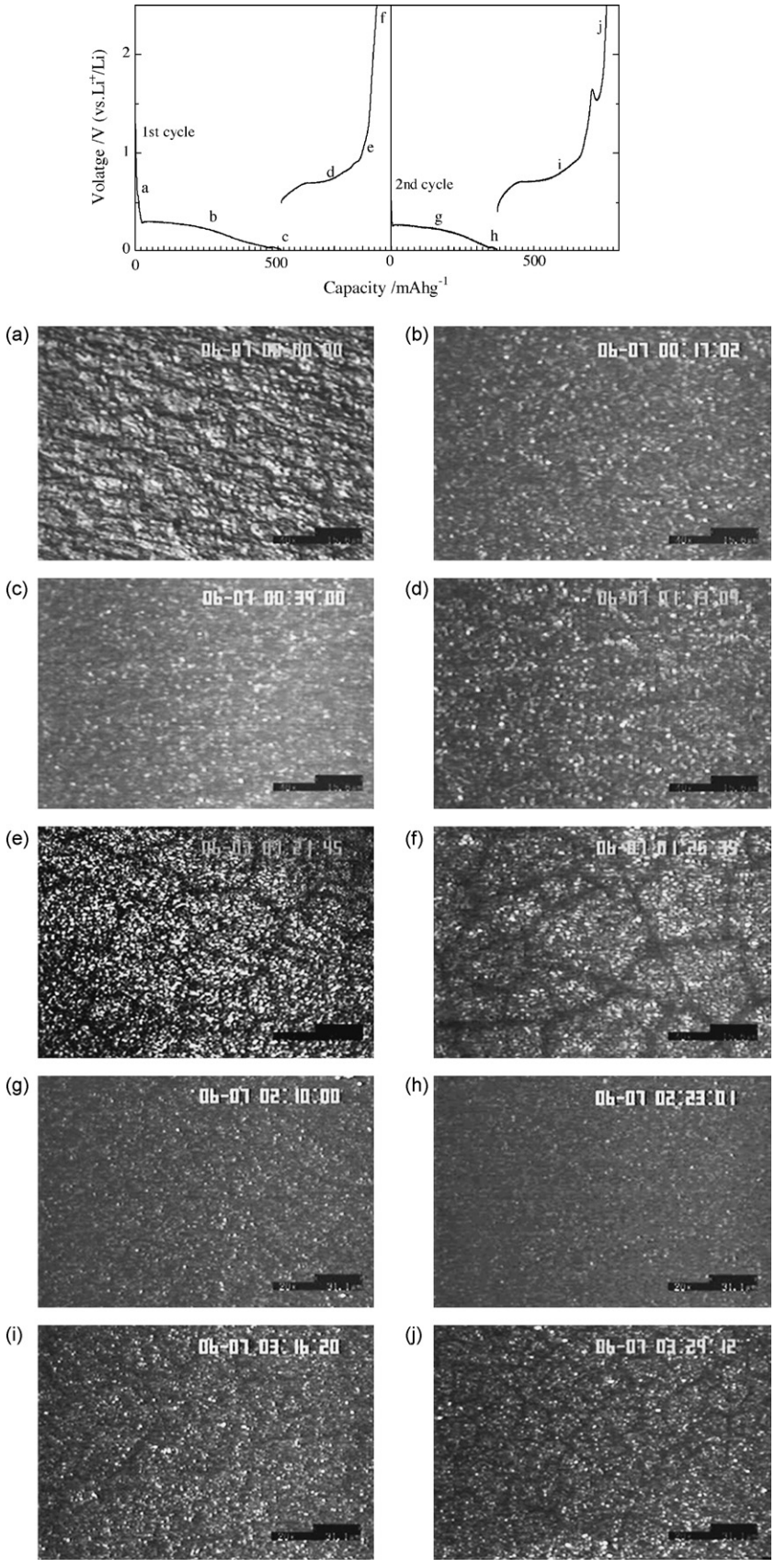

Fig. 3. Charge/discharge curves of a Ni–Sn alloy electrode (top) and LSCM images corresponding to various stages of lithiation as indicated by (a–j) in the charge/discharge curves.

1 h in order to relax the concentration gradient near the Ni–Sn alloy electrode.

The discharging operation was then started. Careful observation reveals the occurrence of cracks in the electrode surface as demonstrated in Fig. 3(d). These cracks are not observed uniformly over the electrode surface. More cracks are observed near the edge of the electrode because shape distortion due to the internal contraction of the active material is concentrated near the edge of the electrode. If a uniform current distribution is assumed over the electrode surface at the very instant of crack formation, a liquid-phase concentration of 0.58 M Li^+ is predicted by the transient one-dimensional diffusion model. The physical meaning of such a surface concentration has to be analyzed in further study.

During further discharging, the crack grows as shown in Fig. 3(e and f). After the charge/discharge cycle, the cell was again left at rest for 1 h. During the second charge half-cycle, the active materials in the electrode expand gradually and the crack seems to disappear at point g (Fig. 3(g)). After that, the surface morphology does not essentially change (Fig. 3(h)). During the second discharge, contraction of the active materials again occurs which re-introduces cracks in the electrode. However, the clarity of the image is degraded because the LSCM image becomes dark due to the transition from crystalline Ni–Sn phase before lithiation to non-crystalline lithiated Ni–Sn phase. Much ingenuity is needed to obtain clearer LSCM images, which are necessary for further detailed discussion.

4. Conclusion

Ni–Sn alloy thin-film electrodes produced by electrodeposition were subjected to lithium charge/discharge cycling (lithiation/delithiation) in an electrochemical and optical cell arrangement suitable for in situ holographic interferometry and LSCM. The transient concentration profiles of Li^+ ion during charging and discharging of Ni–Sn alloy were recorded in situ and successfully analyzed. A simple one-dimensional diffusion model was applied, which satisfactorily predicts the development of concentration gradients during charging (lithiation) and discharging (delithiation) of the Ni–Sn alloy electrode in the $LiClO_4$-PC electrolyte solution.

The evolution of surface morphology of the Ni–Sn alloy electrode during lithiation and delithiation was also observed, using in situ LSCM. Formation of cracks in the electrode was observed during the discharging (delithiation) half-cycle which may be ascribed to the active Sn atoms being constricted due to the extraction of Li atoms. Furthermore, the insertion and extraction of Li make the Ni–Sn alloy electrode non-crystalline, whereby the LSCM image becomes gradually unclear. However, it has been shown that in situ observation of surface morphology variation combined with interferometric measurement of the surface concentration of Li^+ ion may contribute significantly to the correlation of practical problems such as excessive volume expansion and crack formation with particular steps in the mechanism of charging and discharging of the alloy electrode. In particular, it has been shown that crack formation occurs in the initial stages of delithiation, while, depending on the level of current applied, cracks appear to be "repaired" during relaxation of charge/discharge and especially the initial stages of re-charging. Thus, crack formation is correlated with high differential volume expansion in the first stage of lithium alloying.

Acknowledgement

The authors would like to thanks Prof. K. Kanamura for his encouragement and suggestions. Part of this work was carried out with financial support of Y.F. by the Ministry of Education, Science and Technology (Project No. 15360402), which is gratefully acknowledged.

References

[1] N. Li, C.R. Martin, B. Scrosati, J. Power Sources 97–98 (2001) 240.
[2] K.D. Kepler, J.T. Vaughey, M.M. Thackeray, J. Power Sources 81–82 (1999) 383.
[3] J.T. Vaughey, K.D. Kepler, R. Benedek, M.M. Thackeray, Electrochem. Commun. 1 (1999) 517.
[4] R. Benedek, M.M. Thackeray, J. Power Sources 110 (2002) 406.
[5] Y. Xia, T. Sakai, T. Fujieda, M. Wada, H. Yoshinaga, J. Electrochem. Soc 150 (2003) A149.
[6] N. Tamura, R. Ohshita, M. Fujimoto, S. Fujitani, M. Kamino, I. Yonezu, J. Power Sources 107 (2002) 48.
[7] L.Y. Beaulieu, K.C. Hewitt, R.L. Turner, A. Bonakdarpour, A.A. Addo, L. Christensen, K.W. Eberman, L.J. Krause, J.R. Dahn, J. Electrochem. Soc 150 (2003) A149.
[8] T.D. Hatchard, J.R. Dahn, J. Electrochem. Soc 151 (2004) A1628.
[9] T.D. Hatchard, M.N. Obrovac, J.R. Dahn, J Electrochem. Soc 152 (2005) A2335.
[10] H. Mukaibou, T. Momma, M. Mohamedi, T. Osaka, J. Electrochem. Soc. 152 (2005) A560.
[11] K. Nishikawa, M. Ota, S. Izuo, Y. Fukunaka, E. Kusaka, R. Ishii, J.R. Selman, J. Solid State Chem. 8 (2004) 174.
[12] M. Ota, S. Izuo, K. Nishikawa, Y. Fukunaka, E. Kusaka, R. Ishii, J.R. Selman, J. Electroanal. Chem. 559 (2003) 175.
[13] K. Nishikawa, Y. Fukunaka, T. Sakka, Y.H. Ogata, J.R. Selman, J. Electroanal. Chem. 584 (2005) 63.
[14] K. Nishikawa, Y. Fukunaka, T. Sakka, Y.H. Ogata, J.R. Selman, Electrochim. Acta, in press.
[15] A. Timmons, J.R. Dahn, J. Electrochem. Soc. 153 (2006) A1206.